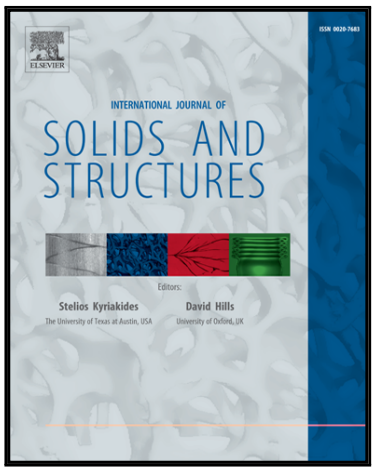

Large Deflections of an Elastic Rod in Contact with a Flat Wall

Milan Batista

PII: S0020-7683(17)30086-0
DOI: 10.1016/j.ijsolstr.2017.02.030
Reference: SAS 9499

To appear in: *International Journal of Solids and Structures*

Received date: 25 July 2016
Revised date: 23 December 2016
Accepted date: 17 February 2017

Please cite this article as: Milan Batista , Large Deflections of an Elastic Rod in Contact with a Flat Wall, *International Journal of Solids and Structures* (2017), doi: 10.1016/j.ijsolstr.2017.02.030

25/11/2013 17:29

Large Deflections of an Elastic Rod in Contact with a Flat Wall

Milan Batista
University of Ljubljana, Faculty of Maritime Studies and Transport
Pot pomorščakov 4, 6320 Portorož, Slovenia
milan.batista@fpp.uni-lj.si

Abstract

This paper presents an analytical solution of two types of contact between an elastic rod and a flat frictionless rigid wall. The first problem deals with large deflections of a rod with one end clamped and the other end pushing towards the clamped end by the wall. The second problem deals with the deflections of a rod that is pushed between fixed wedges. The solutions of both problems are given in terms of Jacobi elliptic functions. The solutions are illustrated using several examples, including deformed rod shapes and load-deflection paths.

Key words. Elasticity, Large deflections, Elastica, Contact problems

1 Introduction

In this paper, we discuss the large deformation of an isotropic and homogeneous Bernoulli–Euler rod (Antman 2005) in contact with an inclined frictionless rigid wall(s). We consider two cases (Fig 1.). In the first case, one end of the rod is clamped and the other end pushes towards the clamped end by the wall. In the second case, the free rod is pushed between fixed walls (wedges). We emphasize that the second problem is different from the problem of squeezing the free rod between movable walls, that is, it is a special case of the first problem. However, if the walls are frictionless, then squeezing of the rod between walls is not possible since there is no applied vertical force that will prevent the rod from sliding up the walls. In both problems, there may be a point and a line contact between the rod and the wall. Therefore, the first problem differs from the classical cantilever problem, and the second differs from the well-known three-point bending problem (Frisch-Fay 1962). For possible

practical applications of these problems in robotics and neuroscience, see the paper by Goss and Chaouki (Goss and Chaouki 2016) and the references given therein.

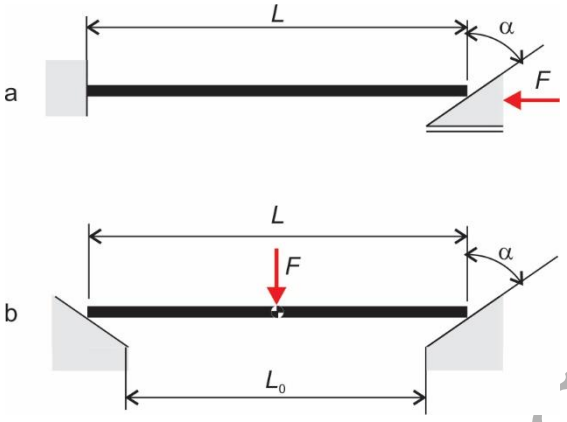

Figure 1. Problem geometry and load.

The literature on the aforementioned problems is relatively new. The first problem was analytically and experimentally discussed by Goss and Chaouki (Goss and Chaouki 2016). They presented an analytical solution of the problem in terms of elliptical integrals for the range $0 \le \alpha < 90^0$. The second problem were treated by Pandit and Srinivasan (Pandit and Srinivasan 2015) using numerical methods.

In this article, we present analytical solutions for both problems in terms of Jacobi elliptic functions. We first review the general solution of the large deflection of the elastica (Batista 2014) and then specialize this solution to the present problems by imposing appropriate boundary conditions. In this way, we reduce each problem to algebraic problems. For all calculations, we use the program Maple. All calculated values are rounded off to six decimal places.

2 Basic equations

We consider an initially straight, inextensible elastic cantilever of length ℓ and bending stiffness $EI > 0$ subject to an end force *R* (see Fig 2). In the Cartesian coordinate system *Oxy*, the shape of the deformed base curve of the cantilever is described by the following differential equations (Antman 2005, Batista 2014):

$$\frac{dx}{ds} = -\cos\phi \qquad \frac{dy}{ds} = -\sin\phi \qquad \frac{d\phi}{ds} = -\kappa \qquad \frac{d\kappa}{ds} = \omega^2 \sin(\phi + \alpha) \tag{1}$$

where $x(s)$ and $y(s)$ are the coordinates of the base curve, $\phi(s)$ is the angle between tangent to the base curve and the *x*-axis, $\kappa(s)$ is the base curve curvature, α is the angle between the *x* axis and the applied force *R*, and $s \in [0,1]$ is the normalized arc length parameter measured from the free cantilever end to the clamped cantilever end. ω is the load parameter defined by

$$\omega^2 \equiv \frac{R\ell^2}{EI} \tag{2}$$

where EI is the cantilever bending stiffness. The solution of (1), subject to the condition that the clamped cantilever end is at the origin, is given by the following functions (Batista 2014):

$$x = \ell\,\hat{x}(s;\omega,k,\alpha), \quad y = \ell\,\hat{y}(s;\omega,k,\alpha) \tag{3}$$

where

$$\begin{aligned} \hat{x}(s;\omega,k,\alpha) &\equiv \hat{\xi}(s;\omega,k)\cos\alpha + \hat{\eta}(s;\omega,k)\sin\alpha \\ \hat{y}(s;\omega,k,\alpha) &\equiv -\hat{\xi}(s;\omega,k)\sin\alpha + \hat{\eta}(s;\omega,k)\cos\alpha \end{aligned} \tag{4}$$

$$\begin{aligned} \hat{\xi}(s;\omega,k) &\equiv \left(\frac{2E(k)}{K(k)} - 1\right)(1-s) + \frac{2}{\omega}\left[Z(\omega + K(k),k) - Z(\omega s + K(k),k)\right] \\ \hat{\eta}(s;\omega,k) &\equiv -\frac{2k}{\omega}\left[\mathrm{cn}(\omega + K(k),k) - \mathrm{cn}(\omega s + K(k),k)\right] \end{aligned} \tag{5}$$

k is the elliptic modulus; $K(k)$ and $E(k)$ are the complete elliptic integrals of the first and second type, respectively (Carlson 2010); *cn*, and Z are Jacobi elliptic functions (Reinhardt and Walker 2010).. The angle ϕ between the tangent to the rod base curve and *x*-axis, and the rod curvature κ are given as follows:

$$\phi = \hat{\phi}(s;\omega,k,\alpha) \equiv 2\sin^{-1}\left[k\,\mathrm{sn}(\omega s + K(k),k)\right] - \alpha \tag{6}$$

$$\kappa = \ell^{-1}\hat{\kappa}(s;\omega,k) \tag{7}$$

where $\hat{\kappa}(s;\omega,k) \equiv 2\omega k\,\mathrm{cn}(\omega s + K(k),k)$ and *sn* is Jacobi elliptic function. The following are the cantilever boundary conditions

$$\hat{x}(1;\omega,k,\alpha)=0\,,\quad \hat{y}(1;\omega,k,\alpha)=0\,,\quad \hat{\kappa}(0;\omega,k)=0 \tag{8}$$

$$\hat{\phi}(1;\omega,k,\alpha)=0 \tag{9}$$

The conditions in Eq. (8) are automatically satisfied by Eqs. (3) and (7), while the condition in Eq. (9) yields the following relation between ω, k, and α.

$$\sin\frac{\alpha}{2}=k\,\mathrm{sn}\left(\omega+\mathrm{K}(k),k\right) \tag{10}$$

Thus, the shape of the rod base curve is completely known when two of the three parameters ω, k, and α are given. In the following discussion, we shall assume that the conditions listed below hold for these parameters:

$$R\geq 0\,,\quad 0\leq k\leq 1,\ -\pi\leq\alpha\leq\pi \tag{11}$$

The first assumption assures that ω is real (see Eq. (2)) and that a unilateral contact exists between the rod and the wall. The remaining two assumptions exclude the symmetric solution from the consideration (Batista 2014).

When $k\neq 0$, we can solve Eq. (10) for ω. The equation has infinite solutions (modes). However, we will consider only the first mode, namely, the only mode that is stable (Batista 2015). Then, the solution of Eq. (10) is as follows:

$$\omega=\hat{\omega}(k,\alpha)\equiv K(k)-\mathrm{sn}^{-1}\left(k^{-1}\sin\frac{\alpha}{2},k\right)\quad (k\neq 0) \tag{12}$$

When $k=0$, Eq. (10) implies $\alpha=0$, which means that the beam is straight and that ω is indeterminate. On the other hand, when $\alpha=0$, Eq. (10) is fulfilled if $k=0$ or if $\mathrm{sn}\left(\omega+K(k),k\right)=0$. The first case has already been considered, while the second is satisfied by $\omega=K(k)$. In the special case that $\omega=K(0)=\pi/2$, from Eq. (2), we obtain the well-known Euler's critical force F_E that bends the initially straight rod

$$\frac{F_E\ell^2}{EI}=\frac{\pi^2}{4} \tag{13}$$

The solution (12) yields a real value only if the following holds:

$$\left|k^{-1}\sin\frac{\alpha}{2}\right|\le 1 \tag{14}$$

We now consider the limit cases of this inequality. When $\alpha>0$ and $k=\sin\frac{\alpha}{2}$, then from Eq. (10), we have $\omega=0$. Further, from Eq. (2), we have $R=0$, while Eq. (3) reduces to $x=\ell(1-s)$ and $y=0$, which are equations for straight lines. When $\alpha<0$, because of the assumption in Eq. $(11)_2$, we obtain $k=-\sin\frac{\alpha}{2}$. From Eq. (10), we obtain $\omega=2K(k)$ for this case.

In the following discussion, we will use the above formulas for solving the present problems. Our assumption that the contact between the rod and the wall is frictionless implies that the reaction force between the rod and the wall is perpendicular to the wall. In other words, for both problems, α is equal to the wall inclination angle. Therefore, for both problems, the only unknown left is *k*, which should be calculated from the specific boundary conditions.

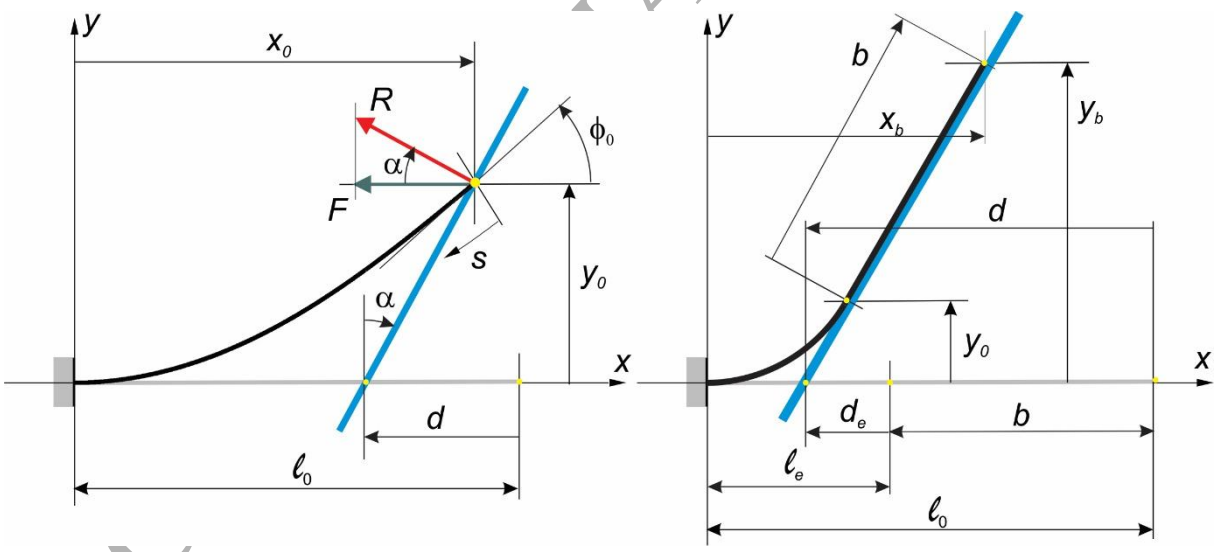

Figure 2. Wall problem geometry and load

3 The cantilever pushed by the wall

We consider an initially straight cantilever rod of length $L=\ell_0$ that is subjected to pressure by the wall (see Fig 2). Two geometrical conditions must be satisfied:

- The free end point of the rod must satisfy the equation of the wall boundary.

$$y = \left[x - \left(\ell_0 - d \right) \right] \cot \alpha \tag{15}$$

where $0 \le d < \ell_0$ is wall displacement, and $|\alpha| < \pi/2$ is the plane inclination angle.

- The tangent angle $\phi_0(\omega, k, \alpha) \equiv \hat{\phi}(0; \omega, k, \alpha)$ at the point of contact of the rod with the wall is bound as shown below.

$$\phi_0(\omega, k, \alpha) \le \frac{\pi}{2} - \alpha \tag{16}$$

To fulfil the first condition, we substitute Eq. (3) for $s = 0$ into Eq. (15) and use ω from Eq. (12). This yields the following expression for wall displacement.

$$d = \ell_0 \hat{d}(k, \alpha), \quad (k \ne 0) \tag{17}$$

where

$$\hat{d}(k, \alpha) \equiv 1 - \hat{x}_0(k, \alpha) + \hat{y}_0(k, \alpha) \tan \alpha = 1 - \frac{\hat{\xi}_0(k, \alpha)}{\cos \alpha} \tag{18}$$

and

$$\hat{x}_0(k, \alpha) \equiv \hat{x}(0; \hat{\omega}(k, \alpha), k), \quad \hat{y}_0(k, \alpha) \equiv \hat{y}(0; \hat{\omega}(k, \alpha), k) \tag{19}$$

$$\hat{\xi}_0(k, \alpha) \equiv \hat{\xi}(0; \hat{\omega}(k, \alpha), k) \tag{20}$$

Formula (17) is valid for any k and α for which Eq. (12) for ω is valid. From the second condition in Eq. (16), we obtain the upper limit of k by using Eq. (6) for ϕ.

$$k \le k_* \equiv \sin \frac{\pi}{4} \tag{21}$$

Note that this upper limit and the condition in Eq. (14) together imply $|\alpha| \le \pi/2$, as already assumed in Eq. (15).

Now, let

$$d_* = \ell_0 \hat{d}_*(\alpha) \tag{22}$$

where

$$\hat{d}_*(\alpha) \equiv \hat{d}(k_*, \alpha). \tag{23}$$

For $d \le d_*$, the contact between the rod and wall is a point. In the limiting case, when $k = k_*$ and $\alpha = \pi/2 - \varepsilon$, where $\varepsilon \ll 1$, we have $\omega = \sqrt{2\varepsilon} + O\left(\varepsilon^{5/2}\right)$ and $d_* = 2/3 + O\left(\sqrt{\varepsilon}\right)$. This limiting value was also obtained by Goss and Chaouki (Goss and Chaouki 2016).

When $d > d_*$, the contact between the rod and wall is a line. In other words, a part of length $0 \le b < \ell_0$ of the free end of the rod slides over the wall. Therefore, the effective length of the beam decreases from ℓ_0 to ℓ_e, whereas the end point of the reduced rod, that is, the elastica of the rod, remains tangent to the wall. In this case, the following geometry relations hold (Fig 2):

$$\ell_e = \ell_0 - b \tag{24}$$

$$d_e = d - b \tag{25}$$

Furthermore, from Eq. (22), we have the following relation.

$$\hat{d}_*(\alpha) = \frac{d_*}{\ell_0} = \frac{d_e}{\ell_e} \tag{26}$$

From Eqs. (25) and (26), we can express wall displacement as a function of rod free length *b* as follows:

$$d = d_* + b\left[1 - \hat{d}_*(\alpha)\right] \tag{27}$$

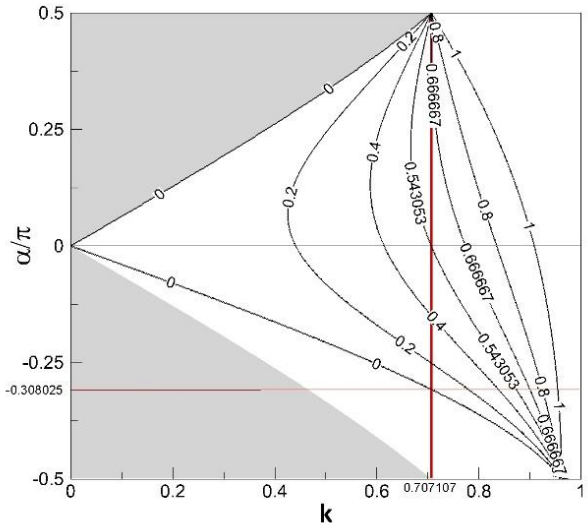

Figure 3. Coontour plot of d/ℓ_0. The vertical line at $k = \sqrt{2}/2$ represents the limit between the rod point and line contact with the wall. For $\alpha \ge 0$, point contact is possible only if

$0 \le d/\ell_0 < 2/3$. For $-0.308025 \le \alpha/\pi < 0$, point contact is possible only if $0 \le d/\ell_0 < 0.543053$. For $\alpha/\pi < -0.308025$, point contact is impossible.

When α is given, Eqs. (17), (22), and (26) give the displacement *d* of the wall as a function of *k* and *b*. When *d* is an independent parameter, three distinct cases are considered.

- When $d < d_*$, we must solve Eq. (17) for the unknown *k* to seek solution in the interval $\left|\sin\frac{\alpha}{2}\right| < k < k_*$ (Fig 3).
- When $d = 0$ and $\alpha > 0$, we have a straight line solution with $k = \sin\frac{\alpha}{2}$ and $\omega = 0$, while for $\alpha = 0$, the solution is $k = 0$ where ω is undetermined.
- When $d \ge d_*$, then $k = k_*$ and $\omega = \omega_*$, while the effective rod length ℓ_e and rod free length *b* are obtained by using Eqs. (24), (25), and (26) as follows:

$$\ell_e = \frac{\ell_0 - d}{1 - \hat{d}_*(\alpha)} \tag{28}$$

$$b = \ell_0 - \ell_e = \frac{d - d_*}{1 - \hat{d}_*(\alpha)} \tag{29}$$

The coordinates of the deformed rod base curve are calculated by using Eq. (3), where for $d \le d_*$, we have $\ell = \ell_0$, and for $d > d_*$, we have $\ell = \ell_e$. In the last case, the coordinates of the end point of the rod are as follows:

$$x_b = \ell_e \hat{x}(0; \omega_*, k_*, \alpha) + b\sin\alpha \qquad y_b = \ell_e \hat{y}(0; \omega_*, k_*, \alpha) + b\cos\alpha \tag{30}$$

We now calculate the pushing force *F* and reaction force *R*. Once *R* is known, we can calculate *F* from (Fig 2)

$$F = R\cos\alpha \tag{31}$$

We note that the unilateral contact condition $R \ge 0$ according to Eq. (31) implies that $F \ge 0$ for $|\alpha| < \pi/2$. Now *R* is given by Eq. (2). When $d \le d_*$, then

$$\frac{R\ell_0^2}{EI} = \hat{\omega}(k, \alpha)^2 \tag{32}$$

.

In the limiting case $d = d_*$ we have $\frac{R_* \ell_0^2}{EI} = \omega_*^2$ where

$$\omega_* = \hat{\omega}_*(\alpha) \equiv \hat{\omega}(k_*, \alpha). \tag{33}$$

When $d > d_*$, because ℓ_0 decreases to ℓ_e, we have $\frac{R\ell_e^2}{EI} = \omega_*^2$. From the identity $\frac{R\ell_e^2}{EI} = \frac{R\ell_0^2}{EI}\left(\frac{\ell_e}{\ell_0}\right)^2$, we obtain the following relation:

$$\frac{R\ell_0^2}{EI} = \left(\frac{\ell_0 \omega_*}{\ell_e}\right)^2 \tag{34}$$

Thus, this problem is solved. Note that in the above formulas, ℓ_0 play the role of a scale factor; hence, in all calculations, we consider $\ell_0 = 1$.

Examples of calculations based on the above formulas are shown in Fig 4, Fig 5, and Fig 6, where the deformed rods for several cases are shown. Some reference numerical values are presented in Table 1, Table 2, and Table 3. Note that the calculated value $F/F_E = 0.76355$ for the case with $\alpha = 30^0$ and $d = d_*$ (Table 1) agrees exactly with value given by Goss and Chaouki (Goss and Chaouki 2016)(Table 1), thus verifying the accuracy of the solution. Further, Fig 7 and 8 present load deflection diagrams.

An interesting case that can be observed in Fig 8 is the case when $d = 0$, and α becomes negative. Let $\alpha = -\varepsilon$, where $\varepsilon \ll 1$, and $k = k_1\varepsilon + k_2\varepsilon^2 + \cdots$ By substituting this expansion into Eq. (12), we consider the limit $\varepsilon \to 0$ to obtain $\omega \to f(k_1)$. The value of coefficient k_1 is calculated from $\hat{d}(k, -\varepsilon) = 0$. The convergence of the solution is presented in Table 4. As seen from the values in the table, the force needed to bend the rod when the wall is slightly negatively inclined is approximately twice the force needed to bend the rod when the wall is slightly positively inclined. In other words, this result shows that bending the rod downwards (towards negative alpha) is impossible from the initial straight configuration since the force needed is higher than the one needed to bend it upwards (towards positive alpha). If we want beam to bend downhill then the rod must already be slightly bent, as is well known from experience.

At the end of this section we conclude that the results for $\alpha > 0$ are the same as those given by Goss and Chaouki (Goss and Chaouki 2016) using elliptic integrals. For $\alpha < 0$, we analytically confirm that this case can be realized only if a rod is initially slightly bent. In addition, for this case, the point of contact is possible only for $0 \le d/\ell_0 < 0.543053$ and $0 > \alpha \ge -55.44^0$. For $\alpha < -55.44^0$, the point of contact is impossible.

Table 1. Calculated values for the rod shapes shown in Fig 4 for which $\alpha = 30^0$. Here, x_0 and y_0 are the coordinates of the end point of the elastica part of the rod, and $F_E \equiv \pi EI/2\ell_0^2$ is Euler critical force.

d/ℓ_0	k	ω	ϕ_0 (°)	x_0/ℓ_0	y_0/ℓ_0	b/ℓ_0	F/F_E
0.4	0.589338	1.282592	42.220039	0.862807	0.455196	0	0.577388
0.619918*	$\sqrt{2}/2$	1.474942	60	0.731206	0.608164	0	0.763555
0.8	$\sqrt{2}/2$	1.474942	60	0.384762	0.320017	0.473798	2.757630

* $d = d_*$

Table 2. Calculated values for the rod shapes shown in Fig 5 for which $\alpha = -30^0$. Here, x_0 and y_0 are the coordinates of the end point of the elastica part of the rod, and $F_E \equiv \pi EI/2\ell_0^2$ is Euler critical force.

d/ℓ_0	k	ω	ϕ_0 (°)	x_0/ℓ_0	y_0/ℓ_0	b/ℓ_0	F/F_E
0	0.408081	2.338602	78.168710	0.615088	0.666686	0	1.919567
0.374910*	$\sqrt{2}/2$	2.233208	120	0.174157	0.781038	0	1.750448
0.6	$\sqrt{2}/2$	2.233208	120	0.111445	0.499792	0.360092	4.274783

* $d = d_*$

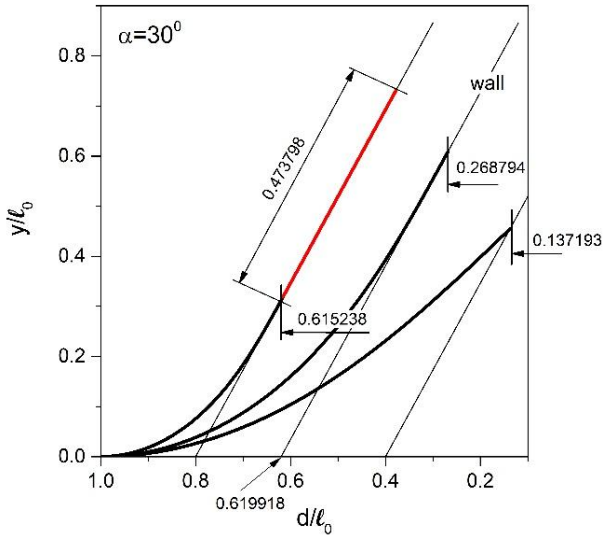

Figure 4. Shape of the rod for the case with $\alpha = 30^0$ for various values of *d*. The dimensons corespond to the displacement of the end point of the rod.

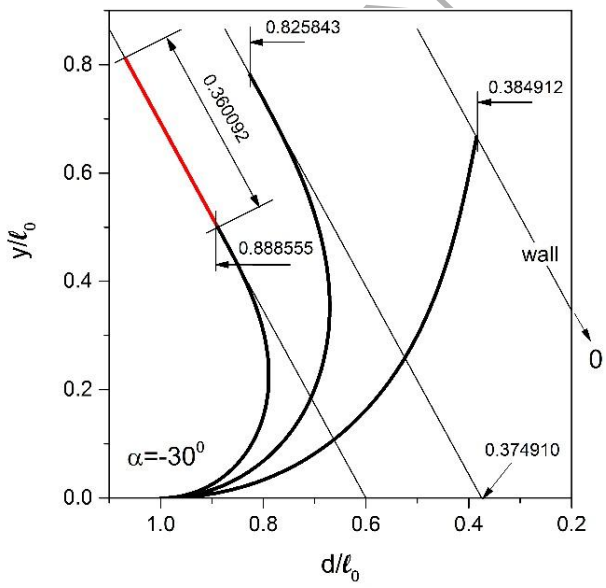

Figure 5. Rod shapes for the case with $\alpha = -30^0$ for various values of *d*. The dimensons corespond to the displacement of the end point of the rod.

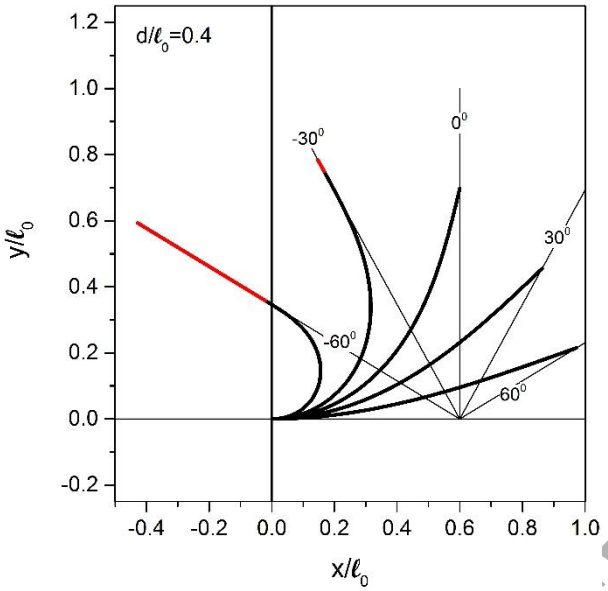

Figure 6. Various beam shapes for $d/\ell_0 = 0.4$ and different values of α.

Table 3. Data for the shapes shown in Fig 6 for which $d/\ell_0 = 0.4$. Here, x_0 and y_0 are the coordinates of the end point of the elastica part of the rod, and $F_E \equiv \pi EI/2\ell_0^2$ is Euler critical force.

α (°)	k	ω	ϕ_0 (°)	x_0/ℓ_0	y_0/ℓ_0	b/ℓ_0	F/F_E
-60	$\sqrt{2}/2$	2.680093	150	-0.021200	0.358650	0.470187	5.185423
-30	$\sqrt{2}/2$	2.233208	120	0.167167	0.749689	0.040138	1.899903
0	0.614552	1.762346	75.838767	0.600000	0.697425	0	1.258759
30	0.589338	1.282592	42.220039	0.862807	0.455196	0	0.577388
60	0.634302	0.822616	18.736438	0.971805	0.214661	0	0.137128

Table 4. Convergence of the solution for $d = 0$ and $\alpha \to 0^-$

No. of terms	k_1	ω	F/F_E
4	0.803068	2.233634	2.022015
8	0.799407	2.245891	2.044267
12	0.799240	2.246632	2.045617
16	0.799226	2.246697	2.045735
20	0.799225	2.246704	2.045748

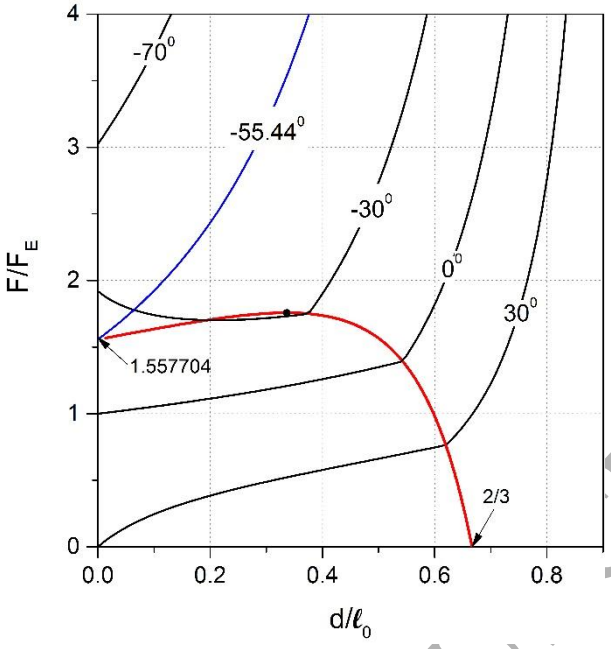

Figure 7. Load deflection diagram of the rod for various inclination angles of the wall. The red (bold) line is the limit between point contact and line contact of the rod with the wall. The limit is maximum for $d/\ell_0 = 0.336546$ and $\alpha = -34.184112^0$ where $F/F_E = 1.757125$.

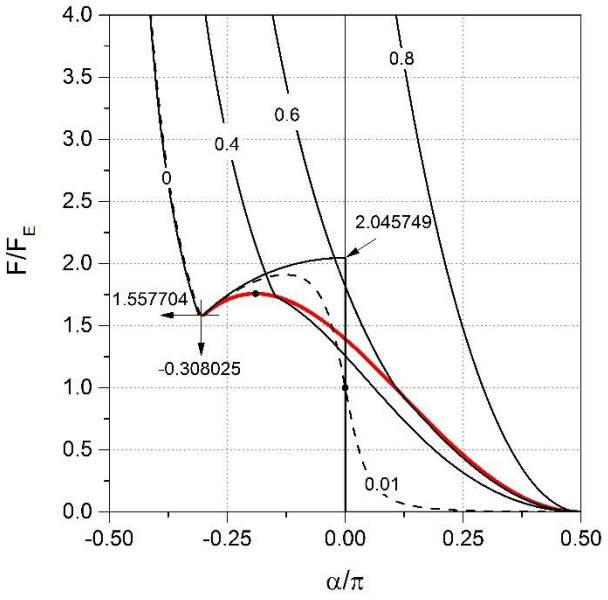

Figure 8. Load deflection diagram of the rod for various wall displacements. The red (bold) line is the limit between point contact and line contact of the rod with the wall. The limit is maximum at $\alpha/\pi = -0.189912$ for which $F/F_E = 1.757125$ and $d/\ell_0 = 0.336546$.

4 Rod pushing between fixed wedges

We now consider the problem of a rod of length $L = 2\ell_0$ pushed between fixed frictionless wedges with a given applied force F (Fig 9). We assume that the problem is symmetric so that we can use the cantilever solution given in the second section.

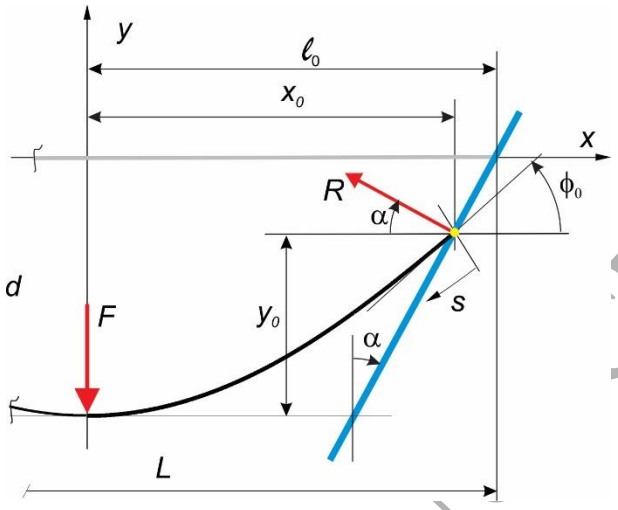

Figure 9. Wedge problem geometry and load

The two geometric constraints of the problem are as follows:

- The contact point must be on the wedge boundary

$$y = (x - \ell_0)\cot\alpha,\ 0 < \alpha < \pi/2 \tag{35}$$

- The contact angle is limited as shown below:

$$\phi_0 \le \pi/2 - \alpha \tag{36}$$

When the wedges form a closed region, that is, if $L_0 = 0$, where L_0 is the distance between the ends of the wedges at the bottom (see Fig 1), the maximum possible deflection is as follows:

$$d_{\max} = \ell_0 \cot\alpha \tag{37}$$

By using condition (35) and Fig 9, we obtain the vertical displacement of the midpoint of the rod

$$d = y_0 + (\ell_0 - x_0)\cot\alpha \tag{38}$$

where x_0 and y_0 are the coordinates of the contact point of the rod. If we substitute Eq. (3) for $s=0$ in this relation and use ω from Eq. (12), we obtain the following relation:

$$d = \ell_0 \hat{d}(k,\alpha) \tag{39}$$

where

$$\hat{d}(k,\alpha) \equiv \hat{y}_0(k,\alpha) + \left(1-\hat{x}_0(k,\alpha)\right)\cot\alpha = \cot\alpha - \frac{\hat{\xi}_0(k,\alpha)}{\sin\alpha} \tag{40}$$

and $\hat{x}_0(k,\alpha)$, $\hat{y}_0(k,\alpha)$, and $\hat{\xi}_0(k,\alpha)$ are given by Eqs. (19) and (20). As in the case of the previous problem, condition (36) implies a point contact between the rod and the wedge for $k \le k_*$ where k_* is given by Eq. (21). When $k = k_*$ we have

$$d_* = \ell_0 \hat{d}_*(\alpha) \tag{41}$$

where $\hat{d}_*(\alpha) \equiv \hat{d}(k_*,\alpha)$. We note that $d_* < d_{\max}$. For $d > d_*$, the contact between the rod and wall is a line, and the free length of the rod reduces from ℓ_0 to ℓ_e. From the geometry, we have relations

$$\ell_e = \ell_0 - b \tag{42}$$

$$d = d_e + \left(\ell_0 - \ell_e\right)\cot\alpha \tag{43}$$

and from Eq. (41), we have

$$\hat{d}_*(\alpha) = \frac{d_e}{\ell_e} = \frac{d_*}{\ell_0}. \tag{44}$$

From Eqs. (42), (43), and (44) we obtain

$$d = d_* + b\left(\cot\alpha - \hat{d}_*(\alpha)\right). \tag{45}$$

Equations (39), (41), and (45) provide the displacement *d* of the midpoint of the rod as a function of *k* and *b* when α is given. When *d* is an independent parameter, then similar to the previous problem, we have three cases.

- When $0 < d < d_*$, we must solve Eq. (39) for an unknown k to seek the solution in the interval $\left|\sin\frac{\alpha}{2}\right| < k < k_*$.
- When $d = 0$, the solution is $k = \sin\frac{\alpha}{2}$ with $\omega = 0$, which means that the rod remains straight.
- When $d \geq d_*$, then $k = k_*$, and $\omega = \omega_*$, while the effective rod length ℓ_e and free length of the rod b are given as shown below, using Eqs. (42), (43), and (44).

$$\ell_e = \frac{\ell_0 \cot\alpha - d}{\cot\alpha - \hat{d}_*(\alpha)} \tag{46}$$

$$b = \frac{d - d_*}{\cot\alpha - \hat{d}_*(\alpha)} \tag{47}$$

The shape of the rod is calculated as follows using Eq. (3):

$$x = \ell\hat{x}(s;\omega,k,\alpha) \qquad y = \ell\hat{y}(s;\omega,k,\alpha) - d \tag{48}$$

where for $d \leq d_*$, we have $\ell = \ell_0$, and for $d > d_*$, we have $\ell = \ell_e$. The coordinates of the end point of the rod are given as follows:

$$x_b = \ell_e\hat{x}(0;\omega_*,k_*,\alpha) + b\sin\alpha \qquad y_b = \ell_e\hat{y}(0;\omega_*,k_*,\alpha) + b\cos\alpha - d\,, \tag{49}$$

Now we will calculate the pushing force F. Owing to the assumption that the contact is frictionless, the reaction force R at the contact point is based on static equilibrium (Batista 2015).

$$R = \frac{F}{2\sin\alpha} \tag{50}$$

From Eq. (2), we have $\frac{R\ell_0^2}{EI} = \hat{\omega}(k,\alpha)^2$. Substituting this into Eq. (50) and considering $L = 2\ell_0$, we obtain the following:

$$\frac{FL^2}{EI} = 8\,\hat{\omega}(k,\alpha)^2\sin\alpha \tag{51}$$

When $d > d_*$ then, since ℓ_0 shrinks to ℓ_e, we have $\frac{R\ell_e^2}{EI} = \omega_*^2$ where ω_* is given by Eq. (33).

From the identity $\omega_*^2 = \frac{R\ell_e^2}{EI} = \frac{R\ell_0^2}{EI}\left(\frac{\ell_e}{\ell_0}\right)^2$ we then obtain the following:

$$\frac{FL^2}{EI} = 8\left(\frac{\ell_0\omega_*}{\ell_e}\right)^2 \sin\alpha \qquad (52)$$

Thus, all the unknowns of the problem become determinate.

Examples of calculations using the above formulas are shown in Fig 10 and Fig 11, and some numerical values are presented in Table 5.

Table 5. Data for the shapes shown in Fig 11 for which $\alpha = 30^0$. Here, x_0 and y_0 are the coordinates of the end point of the elastica part of the rod, and $F_E \equiv \pi EI/2L^2$ is Euler critical force.

d/ℓ_0	k	ω	ϕ_0 (°)	x_0/ℓ_0	y_0/ℓ_0	b/ℓ_0	F/F_E
0.5	0.517894	1.166182	32.328240	0.918154	-0.141762	0	2.204717
1.073729*	$\sqrt{2}/2$	1.474942	60	0.731206	-0.465564	0	3.526711
1.5	$\sqrt{2}/2$	1.474942	60	0.257742	-1.285629	0.647512	28.384448

* $d = d_*$

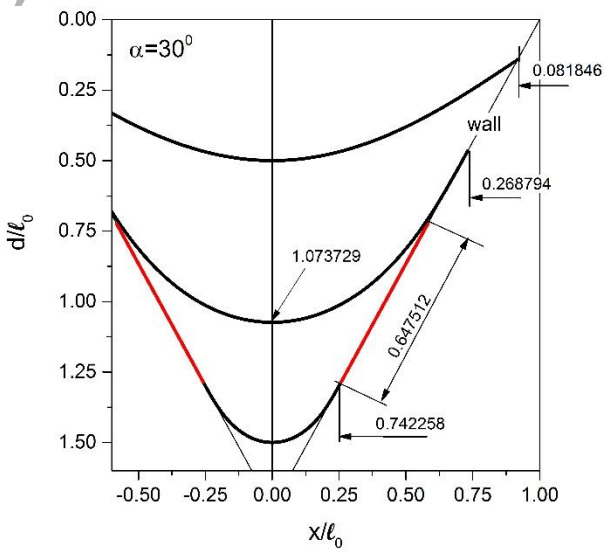

Figure 10. Rod shapes for various midpoint deflections when $\alpha = 30^0$. The dimensons correspond to the displacement of the end point of the rod.

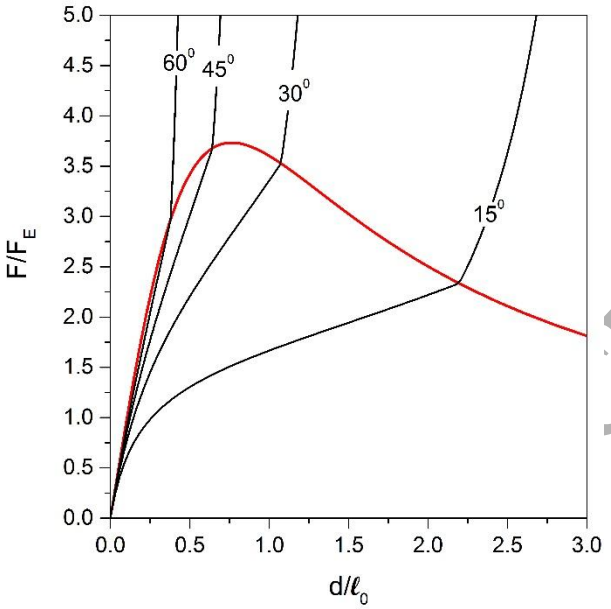

Figure 11. Load deflection diagram for the wedge problem. The red (bold) line is the limit between the point and line contact. The limit is maximum when $d/\ell_0 = 0.763310$ and $\alpha = 39.757754^0$ for which $F/F_E = 3.733578$.

If the wedges do not form a closed region, that is, if $0 < L_0 < L$, then the rod will slip through between wedges when it undergoes sufficient displacement. This situation may arise in two cases. In the first case, the rod will slip through from the wedges when its end points reach the bottom of the wedges, that is, when $x_0 = L_0/2$ (see Fig 12, shape 2). Using Eq. (19), the following equation is obtained from this condition.

$$\hat{x}_0(k_0, \alpha) = \frac{L_0}{L} \tag{53}$$

which can be numerically solved for k_0. Once k_0 is known, using Eq. (39), we can calculate the deflection $d_0 = \ell_0 \hat{d}(k_0, \alpha)$ and the corresponding pushing force by using Eq. (51). If $k_0 \le k_*$, $d_0 \le d_*$, and hence, the rod maintains point contact with the wedges before it pops out. If $k_0 > k_*$, then the rod maintains line contact with the wedges, and the end points of the

elastica part of the rod will reach the bottom of the wedges when the following condition is satisfied:

$$\frac{\ell_e}{\ell_0}\hat{x}_0\left(k_*,\alpha\right)=\frac{L_0}{L} \tag{54}$$

Thus, we can calculate the corresponding midpoint displacement d_0 by using Eqs. (45), (46), and (47):

$$d_0=\ell_0\left[\cot\alpha-\left(\frac{L_0}{L}\right)\frac{\cot\alpha-\hat{d}_*\left(\alpha\right)}{\hat{x}_0\left(k_*,\alpha\right)}\right] \tag{55}$$

This limit situation is shown in Fig 13, shape 1. When the displacement increases further, that is, $d>d_0$, a three-point-bending problem arises (Batista 2015); then, the inclination angle of the end point of the rod $\alpha'=\pi/2-\phi_0$ decreases from α to zero. In other words, the line contact between the rod and the wedges is lost, and a point contact is formed at the bottom of the wedges. The unknown in the three-point-bending problem is the effective rod length, which is given using Eq. (54) as follows:

$$\ell'_e=\ell_0\frac{1}{\hat{x}_0\left(k_*,\alpha'\right)}\left(\frac{L_0}{L}\right) \tag{56}$$

Alternatively, we can express the three-point bending problem in terms of the deflection of the midpoint of the rod the end point of the elastic part of the rod is at the bottom of the wedges, the following relation holds:

$$\ell'_e\hat{y}_0\left(k_*,\alpha'\right)=d-\ell_0\left(1-\frac{L_0}{L}\right)\cot\alpha \tag{57}$$

This can be numerically solved for α' when *d* is given.

Now, the rod will slip through between the wedges when $\alpha'=0$, i.e. when $R=0$ or when $\ell'_e=1$(see Fig 13, shape 2). When $\alpha'=0$ the maximal displacement is expressed as follows using Eq. (57).

$$d_{\max} = \ell_0 \left[\cot\alpha + \frac{L_0}{L} \left(\frac{\hat{y}_0(k_*, 0)}{\hat{x}_0(k_*, 0)} - \cot\alpha \right) \right] \tag{58}$$

When $\ell'_e = 1$, then $\alpha'_{\min} > 0$ and the maximum displacement is given using Eq. (57):

$$d_{\max} = \ell_0 \left[\hat{y}_0(k_*, \alpha'_{\min}) + \left(1 - \frac{L_0}{L} \right) \cot\alpha \right] \tag{59}$$

where $\alpha'_{\min} > 0$ is numerically calculated using the following expression:

$$\hat{x}_0(k_*, \alpha'_{\min}) = L_0 / L \tag{60}$$

Condition $\ell'_e = 1$ will be attained before condition $\alpha' = 0$ if the hole is sufficiently large, i.e. if $L_0/L > \hat{x}_0(k_*, 0) = 0.456947$. The difference between these conditions can be observed in Fig 12 and Fig 13, which show the rod shapes for $d = d_0$ and $d = d_{\max}$.

Table 6. Data for the rod shapes shown in Fig 12 for which $\alpha = 30^0$ and $L/L_0 = 2$.

Shape	d/ℓ_0	k	ω	ϕ_0 (°)	x_0/ℓ_0	y_0/ℓ_0	b/ℓ_0	F/F_E
1*	1.281889	$\sqrt{2}/2$	1.474942	60	0.5	-0.866025	0.316198	7.542402
2**	1.614345	$\sqrt{2}/2$	1.799079	85.546027	0.5	-0.866025	0	0.547756

* $d = d_0$ ** $d = d_{\max}$

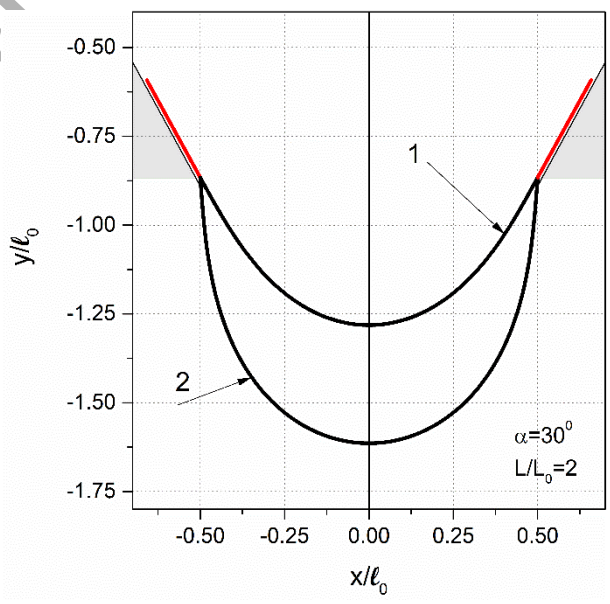

Table 12. Deformed rod shapes for $\alpha = 30^0$ and $L/L_0 = 2$.

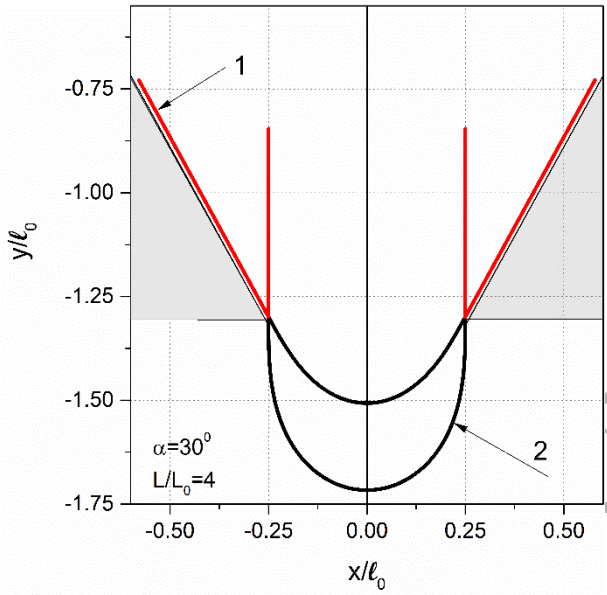

Table 13. Deformed rod shapes for $\alpha = 30^0$ and $L/L_0 = 4$.

Table 7. Data for rod shapes shown in Fig 13 for which $\alpha = 30^0$ and $L/L_0 = 4$.

Shape	d/ℓ_0	k	ω	ϕ_0 (°)	x_0/ℓ_0	y_0/ℓ_0	b/ℓ_0	F/F_E
1*	1.506970	$\sqrt{2}/2$	1.474942	60	0.25	-1.299038	0.658099	30.169606
2**	1.716352	$\sqrt{2}/2$	1.854075	90	0.25	-1.299038	0.452890	0

* $d = d_0$ ** $d = d_{\max}$

Conclusions

In this paper, we show that the general solution for the Bernoulli–Euler rod can be used to obtain solutions for two types of the rod contact problems. For the case in which a cantilever is pushed by the wall, the results agree well with those given in literature (Goss and Chaouki 2016). The present solution, however, covers the wider range of $-90 < \alpha < 90^0$. To the best of our knowledge, the analytical results for the case of a rod being pushed between fixed wedges are new.

As mentioned in the Introduction, squeezing of the free rod between frictionless walls was not possible because an applied force was needed to prevent the rod from popping out of the walls. Thus, an interesting and open question would be how to treat such squeezing between frictional walls.

References

Antman, S. S. (2005). Nonlinear problems of elasticity. New York, Springer.
Batista, M. (2014). "Analytical treatment of equilibrium configurations of cantilever under terminal loads using Jacobi elliptical functions." International Journal of Solids and Structures **51**(13): 2308-2326.
Batista, M. (2015). "Large deflections of a beam subject to three-point bending." International Journal of Non-Linear Mechanics **69**: 84-92.
Batista, M. (2015). "A simplified method to investigate the stability of cantilever rod equilibrium forms." Mechanics Research Communications **67**: 13-17.
Carlson, B. C. (2010). Elliptic Integrals. F. W. J. Olver and National Institute of Standards and Technology (U.S.). Cambridge ; New York, Cambridge University Press : NIST**:** xv, 951 p.
Frisch-Fay, R. (1962). Flexible bars. London, Butterworths.
Goss, V. G. A. and R. Chaouki (2016). "Loading paths for an elastic rod in contact with a flat inclined surface." International Journal of Solids and Structures **88-89**: 274-282.
Pandit, D. and S. M. Srinivasan (2015). Simplified contact analysis for slender beams undergoing large deflection. Proceedings of Indian National Conference on Applied Mechanics INCAM 2015. New Delhi, India. **2:** 16-21.
Reinhardt, W. P. and P. L. Walker (2010). Jacobian Elliptic Functions. NIST handbook of mathematical functions. F. W. J. Olver. Cambridge ; New York, Cambridge University Press : NIST**:** xv, 951 p.